Structure and phase diagram of self-assembled rigid rods: Equilibrium polydispersity and nematic ordering in two dimensions

J. M. Tavares,[1,2] B. Holder,[1] and M. M. Telo da Gama[1,3]
[1]*Centro de Física Teórica e Computacional, Universidade de Lisboa, Avenida Professor Gama Pinto 2, P-1649-003 Lisbon, Portugal*
[2]*Instituto Superior de Engenharia de Lisboa, Rua Conselheiro Emídio Navarro 1, P-1950-062 Lisbon, Portugal*
[3]*Departamento de Física, Faculdade de Ciências, Universidade de Lisboa, Campo Grande, P-1749-016 Lisbon, Portugal*
(Received 15 December 2008; published 20 February 2009)

We investigate the influence of directional or bonding interactions on the structure and phase diagram of complex fluids. Using a generalization of the theory of associating fluids we study the interplay between the self-assembly process, driven by the bonding interactions, and the isotropic-nematic transition, driven by the anisotropic shape of the equilibrium clusters, for a model consisting of particles with two bonding sites and discrete orientational degrees of freedom. The theory is applied over a wide range of temperature and density in two dimensions and the results are compared with Monte Carlo simulations on the square lattice. The specific heat is shown to exhibit pronounced structure at the onset of self-assembly and at the nematic-isotropic transition that occur over a narrow range of temperature, at fixed density. The results reveal that bonding is enhanced by the nematic ordering, although a bonding temperature still occurs in the isotropic phase at low densities. The average rod length is described quantitatively in both phases, while the location of the ordering transition, which was found to be continuous, is predicted semiquantitatively by the theory.

DOI: 10.1103/PhysRevE.79.021505 PACS number(s): 64.75.Yz, 61.20.Ja, 64.70.mf, 82.70.Dd

I. INTRODUCTION

Recently it has become possible to fabricate well-defined colloidal particles with dimensions in the nanometer-to-micrometer range. Unlike in atomic systems, the interactions between colloidal particles may be controlled, providing new windows into structural and thermodynamic behavior [1]. Of particular interest are the so-called patchy colloids, the surfaces of which are patterned so that they attract each other via discrete bonding sites of tunable number, size, and strength. The thermodynamics of bonded self-assembled systems is currently a topic of intense research. On the theoretical side, studies based on the theory of associating fluids [2,3] and computer simulations of simple models have provided a wealth of new results [4–7]. Self-assembled systems are best characterized by a bonding line, in the temperature-density plane, that signals the onset of the bonding process, beyond which the fraction of particles in bonded clusters is significant. This line is defined by the maxima in the specific heat that reveal a rapid change of the internal energy as the bonds are formed. The presence of these maxima is clear, experimentally detectable, evidence of the leading role of bonding interactions in the thermodynamics. In systems with two bonding sites per particle, only (polydisperse) linear chains form and there is no liquid-vapor phase tansition [7]. However, if the chains are sufficiently stiff they may undergo an isotropic-nematic transition, at fixed density, at a temperature close to the bonding temperature.

It is well known that solutions of rodlike particles exhibit a transition from a disordered isotropic phase to an ordered nematic phase as the concentration of rods increases. In the isotropic phase the rods have no preferred orientation, whereas in the nematic phase there is an average alignment of the rods. In 1949, Onsager [8] showed that the ordering could be explained, at least for solutions of monodisperse long thin rigid rods, by considering the competition between the excluded volume of two rods and the orientational entropy. In a system of self-assembled rods, at fixed concentration, an isotropic-nematic transition may be driven by the temperature since the average rod length increases rapidly as the temperature decreases. However, the self-assembled system is intrinsically polydisperse and the generalization of Onsager's approach to this problem is far from trivial.

A related problem arises in the study of suspensions of rigid rods with quenched polydispersity, i.e., systems where the distribution of lengths is predetermined (by preparation) and does not depend on the density and temperature. In a recent study with solutions of natural (polydisperse) rodlike clay particles a strong first-order nematic transition was observed at volume fractions close to 0.06, for rods with length-to-diameter ratio of approximately 27 [9]. The phase volumes and particle concentrations in the coexisting phases were determined and the polydispersity of both daughter phases was found to be distinctly smaller than that of the parent suspension [9]. The dependence of these quantities on the concentration as well as the observation of a second nematic phase were found to be in line with Onsager's theory extended to bidisperse systems [10].

Most studies to date of continuous polydispersity are perturbative [11], limiting the validity of the analysis to situations with narrow distributions of rod lengths that are not guaranteed in self-assembled systems. A different approach to the ordering of monodisperse rodlike mixtures has been proposed by Zwanzig [12]. In this model the orientations of the rods are restricted to be in one of three mutually perpendicular directions in three dimensions. This enables the exact calculation of higher-order virial coefficients and of the orientational distribution functions. In contrast to Onsager's approach, the Zwanzig model is readily extended to polydisperse systems [13] and the polydisperse Zwanzig model provides a useful starting point for understanding the effects of continuous equilibrium polydispersity on the phase behavior of hard rod systems.

In this paper, we consider the isotropic-nematic transition in a system of self-assembled rods as part of the general ongoing effort to develop a deeper understanding of self-assembly. We consider a simple version of the models for patchy colloids used in [4–7]. Each particle is endowed with an orientational degree of freedom that can take on a finite number of values representing the discretized set of orientations of the sticky patches. The interaction strength between two particles depends on their relative orientations and on their orientations relative to the intermolecular vector. This anisotropy of the interactions mimics the fact that two patches on different particles can only stick if they overlap. In the spirit of the Zwanzig model we assume that the intermolecular vector can take only a discrete number of orientations. The theory for the structure and thermodynamics of the self-assembled Zwanzig model is particularly simple and physically transparent allowing us to investigate the interplay between self-assembly and nematic ordering. We use the theory to analyze the full range of temperature and density of a system of particles with two bonding sites in two dimensions and perform lattice Monte Carlo simulations to check the theoretical predictions. In particular, we calculate the response functions and investigate whether a bonding temperature occurs above or below the isotropic-nematic transition.

For the continuum orientational problem, there is general agreement that in three dimensions, infinitely thin rods undergo a first-order isotropic-nematic transition, as pointed out by Onsager, and that polydispersity increases the transition's first-order character [14–16]. By contrast, the nature of the transition in two dimensions has been a topic of active theoretical study over the last three decades and appears to depend crucially on the particle interactions. Early seminal contributions to this subject were made by Straley [17] and Frenkel and Eppenga [18] and continuous polydispersity was considered in [19]. Here, we consider a self-assembled two-dimensional system with discrete orientations that is expected to have a less subtle phase behavior.

Even without self-assembly, however, the lattice version of our model was shown recently to exhibit a number of interesting features [20–22]. It has been shown that (i) nematic order is stable above a minimal size of the rods aspect ratio [20,22]. (ii) The transition is continuous, in the Ising and Potts universality classes for square and triangular lattices, respectively [21]. (iii) On the square lattice the nematic transition is reentrant, as the full lattice is disordered [22].

This paper is organized as follows: In the next section we provide a derivation of the theory and apply it to the self-assembled Zwanzig model in two dimensions. Lattice simulations are described in Sec. III where a detailed comparison with the theoretical predictions is carried out. The results are further discussed in Sec. IV where we summarize our conclusions.

II. SELF-ASSEMBLED ZWANZIG MODEL: THEORETICAL RESULTS

We consider a model for self-assembly in the spirit of the Zwanzig model. The particles have spherical hard cores and interact with nearest neighbors through anisotropic attractive interactions. Each particle possesses a discrete number of orientations, along d mutually perpendicular directions in d dimensions, akin to the discrete orientations of rods in the model proposed by Zwanzig. The bond energy is $-\epsilon$ if two neighboring particles are aligned with each other and with the intermolecular vector and is zero otherwise. A cluster or uninterrupted sequence of bonded particles is a rod in two dimensions. At fixed density, the average rod length increases as the temperature decreases and the polydisperse rods will undergo an ordering transition. In the following we provide a theoretical framework to describe the ordering transition in the self-assembled Zwanzig model.

A polydisperse system of rods in three dimensions with three discrete orientations along three perpendicular directions (polydisperse Zwanzig model) has been investigated theoretically in [13]. Apart from the spatial dimension our model differs from that studied in [13] as it considers equilibrium self-assembly. In the self-assembled Zwanzig model the polydispersity is annealed, rather than quenched, and the rod length and orientational distributions change as the temperature and density change. There are however similarities in the theoretical treatments of these models.

We start by defining $\phi(\ell)$, the density of clusters (rods) with length ℓ, $\phi_\alpha(\ell)$, the density of clusters with length ℓ and orientation α [along the x, y directions in two dimensions (2D)] and ϕ, the total density of clusters. These densities are related through the sum rules,

$$\phi(\ell) = \sum_\alpha \phi_\alpha(\ell), \tag{1}$$

$$\phi = \sum_\ell \phi(\ell). \tag{2}$$

We also define $P_\alpha(\ell)$ as the fraction of clusters of length ℓ with orientation α. These are the discrete orientational distribution functions that are normalized,

$$\sum_\alpha P_\alpha(\ell) = 1, \tag{3}$$

and may be used to write the density of clusters with length ℓ and orientation α as

$$\phi_\alpha(\ell) = \phi(\ell) P_\alpha(\ell). \tag{4}$$

It is useful to define ρ_α, the density of particles in clusters with orientation α and ρ, the total density of particles. The particle densities are related to the cluster density distributions through

$$\rho_\alpha = \sum_\ell \ell \phi_\alpha(\ell), \tag{5}$$

$$\rho = \sum_\ell \ell \phi(\ell), \tag{6}$$

and

$$\rho = \sum_\alpha \rho_\alpha. \tag{7}$$

The free energy per unit volume of an ideal (noninteracting) mixture of clusters with density distributions $\phi_\alpha(\ell)$ (which we will take as the reference system) is

$$\beta f^{\mathrm{ref}} = \sum_\alpha \sum_\ell \phi_\alpha(\ell)[\ln \phi_\alpha(\ell) - 1 - \ln \tilde{q}_\alpha(\ell)], \tag{8}$$

where

$$\tilde{q}_\alpha(\ell) = \exp[(\ell - 1)\beta\epsilon], \tag{9}$$

is the partition function of a cluster of length ℓ and orientation α (divided by the total volume).

The Zwanzig model is treated in the second virial approximation even though, by contrast to the Onsager model, this is not exact in the limit of infinitely long rods [12]. The excess free energy is determined essentially by the excluded volume of a pair of rods [13],

$$\beta f^{\mathrm{exc}} = \frac{1}{2} \sum_{\alpha,\alpha'} \sum_{\ell,\ell'} \phi_\alpha(\ell)\phi_{\alpha'}(\ell')V_{\mathrm{exc}}(\ell,\alpha;\ell',\alpha'), \tag{10}$$

where $V_{\mathrm{exc}}(\ell,\alpha;\ell',\alpha')$ is the excluded volume of two rods, the first with length ℓ and orientation α and the second with length ℓ' and orientation α'. This volume is given by

$$V_{\mathrm{exc}}(\ell,\alpha;\ell',\alpha') = \ell\ell'(1 - \delta_{\alpha,\alpha'}), \tag{11}$$

where we neglected the excluded volume of parallel rods since it is small compared to the excluded volume of perpendicular rods, in the Onsager limit (see [12,13]).

Substituting (11) in (10) we find

$$\beta f^{\mathrm{exc}} = \sum_{\ell,\ell'} \ell\ell' \phi_x(\ell)\phi_y(\ell') = \rho_x\rho_y, \tag{12}$$

a drastic approximation for the excess free energy of the model [23], the simplicity of which will allow us to derive analytic expressions for the thermodynamics and structure of the polydisperse system, in the isotropic and nematic phases. In Sec. III we check its accuracy by comparing the theoretical results with the results of computer simulations.

The equilibrium distributions, $\phi_\alpha(\ell)$, are found by minimizing the total free energy with respect to the orientational distribution functions $P_\alpha(\ell)$ and cluster density distributions $\phi(\ell)$, with the constraints (3) and (6). We introduce Lagrange multipliers, $k_\alpha(\ell)$ and μ, and write

$$\frac{\delta\beta f}{\delta P_\alpha(\ell)} = k_\alpha(\ell), \tag{13}$$

$$\frac{\delta\beta f}{\delta\phi(\ell)} = \ell\beta\mu. \tag{14}$$

The Lagrange multipliers $k_\alpha(\ell)$ are determined by the normalization condition of the orientational distribution functions (3) while μ, the chemical potential, is determined by the sum rule for the total particle density (6). In zero external field, the k_α are independent of α and a straightforward implementation of (3) yields the usual orientational distribution functions [13].

To derive the general equilibrium conditions in 2D it is convenient to write the free energy as

$$\beta f = \sum_{\alpha=x,y} \sum_\ell \phi_\alpha(\ell)[\ln \phi_\alpha(\ell) - 1 - (\ell - 1)\beta\epsilon] + \rho_x\rho_y. \tag{15}$$

Recalling the dependence of ρ_x and ρ_y on ϕ_α, it is easy to show that

$$\frac{\delta\beta f}{\delta\phi_x(\ell)} = \ln \phi_x(\ell) - (\ell - 1)\beta\epsilon + \ell\rho_y \tag{16}$$

and

$$\frac{\delta\beta f}{\delta\phi_y(\ell)} = \ln \phi_y(\ell) - (\ell - 1)\beta\epsilon + \ell\rho_x. \tag{17}$$

Defining the cluster density distribution difference as

$$\delta(\ell) = \phi_x(\ell) - \phi_y(\ell) \tag{18}$$

the minimization of βf with respect to the orientational distribution functions (13), subject to the normalization condition, is equivalent to the minimization of βf with respect to $\delta(\ell)$,

$$\frac{\delta\beta f}{\delta\delta(\ell)} = \ell\beta h, \tag{19}$$

where h is the external field coupled to the orientational density difference, $\rho_x - \rho_y$.

The derivatives of βf with respect to $\phi(\ell)$ and $\delta(\ell)$ are simply related to its derivatives with respect to $\phi_x(\ell)$ and $\phi_y(\ell)$, (16) and (17), and the equilibrium conditions, (14) and (19), become

$$\ell\beta\mu = \tfrac{1}{2}[\ln \phi_x(\ell) + \ln \phi_y(\ell) + \ell\rho] - (\ell - 1)\beta\epsilon, \tag{20}$$

$$\ell\beta h = \tfrac{1}{2}[\ln \phi_x(\ell) - \ln \phi_y(\ell) - \ell(\rho_x - \rho_y)]. \tag{21}$$

The solution of these equations yields the equilibrium cluster density distributions,

$$\phi_x(\ell) = \exp(-\beta\epsilon)[z \exp(\tilde{\Delta})]^\ell, \tag{22}$$

$$\phi_y(\ell) = \exp(-\beta\epsilon)[z \exp(-\tilde{\Delta})]^\ell, \tag{23}$$

where we have defined the quantities,

$$z = \exp\left(\beta(\mu + \epsilon) - \frac{\rho}{2}\right), \tag{24}$$

$$\tilde{\Delta} = \beta h + \frac{\Delta}{2}, \tag{25}$$

$$\Delta = \rho_x - \rho_y. \tag{26}$$

Δ is the order parameter coupled to the external field, h, while z and $\tilde{\Delta}$ are mixed field-density $(\mu - \rho, h - \Delta)$ variables, that are coupled as a result of the equilibrium self-assembly process. We can think of z as the activity of an effective chemical potential, measured with respect to the bonding energy $-\epsilon$ (in units of $k_B T$), minus one-half of the total density, $\frac{\rho}{2}$. Likewise, $\tilde{\Delta}$, is an effective external field given by the

external field h (in units of k_BT), plus one-half of the order parameter, $\frac{\Delta}{2}$.

The equilibrium orientational densities obtained from (22), (23), and (5) are

$$\rho_x = \exp(-\beta\epsilon)\frac{z\exp(\tilde{\Delta})}{[1-z\exp(\tilde{\Delta})]^2}, \tag{27}$$

$$\rho_y = \exp(-\beta\epsilon)\frac{z\exp(-\tilde{\Delta})}{[1-z\exp(-\tilde{\Delta})]^2}, \tag{28}$$

in terms of which all thermodynamic and structural quantities of interest may be determined. In what follows we summarize those that will be used in this study.

(a) *Equations of state*. The density and order-parameter equations of state are obtained by substituting the equilibrium orientational densities, (27) and (28), in the equations for the total density, ρ, (7) and the order parameter, Δ, (26),

$$\rho = \exp(-\beta\epsilon)\left(\frac{z\exp(\tilde{\Delta})}{[1-z\exp(\tilde{\Delta})]^2} + \frac{z\exp(-\tilde{\Delta})}{[1-z\exp(-\tilde{\Delta})]^2}\right), \tag{29}$$

and

$$\Delta = \exp(-\beta\epsilon)\left(\frac{z\exp(\tilde{\Delta})}{[1-z\exp(\tilde{\Delta})]^2} - \frac{z\exp(-\tilde{\Delta})}{[1-z\exp(-\tilde{\Delta})]^2}\right). \tag{30}$$

In all subsequent calculations of equilibrium quantities the equations of state are solved to obtain the equilibrium values of Δ and z, at fixed ρ and T, in zero external field, $h=0$. Note that the order-parameter equation of state (30) has always one solution $\Delta=0$ when $h=0$. In the region where this is the only solution the system is in the isotropic phase. It is straightforward to show that, in zero field, z is an even function of Δ and as a result, at fixed ρ and T, the order-parameter equation of state (30) has either one or three solutions. The pair of nonzero order-parameter equilibrium solutions is symmetrical, ruling out the possibility of a first-order isotropic-nematic transition in the 2D Zwanzig model (within this approximation).

(b) *Free energy and pressure*. The equilibrium free energy follows by substituting the equilibrium cluster density distributions, (22) and (23), into (15),

$$\beta f(T,\rho,\Delta) = \beta\mu\rho + \beta h\Delta - \beta p, \tag{31}$$

where the pressure is given by

$$\beta p = \phi + \frac{\rho^2}{4} - \frac{\Delta^2}{4}. \tag{32}$$

(c) *Average rod length*. The equilibrium average rod length is obtained immediately from

$$\bar{\ell} \equiv \frac{\rho}{\phi} = \frac{1}{1-z\left(\cosh(\tilde{\Delta}) + \frac{2\tilde{\Delta}}{\rho}\sinh(\tilde{\Delta})\right)}, \tag{33}$$

where the equality follows from the calculation of the equilibrium total density of clusters, ϕ, using (22) and (23). In the isotropic phase the average rod length is found by setting $\tilde{\Delta}=0$, and we find

$$\bar{\ell} = \frac{1+\sqrt{1+2\rho\exp(\beta\epsilon)}}{2}, \tag{34}$$

in line with the result for a system of noninteracting self-assembled chains [24,25].

(d) *Cluster density distribution*. The equilibrium total cluster density distribution, $\phi(\ell)$, is obtained from (22) and (23),

$$\phi(\ell) = 2\exp(-\beta\epsilon)z^{\ell}\cosh(\ell\tilde{\Delta}), \tag{35}$$

and, as expected, it is a single exponential in the isotropic phase, $\tilde{\Delta}=0$, while in the nematic phase it is the sum of two exponentials.

(e) *Isotropic-nematic transition line*. The critical isotropic-nematic transition occurs on a line in the (ρ,T) plane, given by

$$\left(\frac{\partial\beta h}{\partial\Delta}\right)_{\rho,h=0} = 0 \tag{36}$$

that after evaluating the derivatives (see the Appendix) becomes

$$\frac{\rho}{2}\frac{1+z}{1-z} = 1. \tag{37}$$

Above this line [in the (ρ,T) plane] the stable phase is isotropic and below it is nematic. Using the equation of state for the total density, (29), the critical line may be written as

$$\exp(\beta\epsilon) = \frac{(2-\rho)(2+\rho)}{2\rho^3}, \tag{38}$$

or, defining the dimensionless temperature as $T^*=k_BT/\epsilon$,

$$T_c^* = \left[\ln\left(\frac{(2-\rho)(2+\rho)}{2\rho^3}\right)\right]^{-1}. \tag{39}$$

The critical line and the equilibrium average rod length at the transition are plotted in Fig. 1, for the whole range of temperature and density. Note that the theory predicts stable nematic phases below the minimal value of the aspect ratio established for monodisperse rods, in 2D simulations [20,22]. In this region of high densities (>0.3) the results of the theory for the nematic phase are not reliable (see below) and higher-order virial approximations or more sophisticated theories are needed to describe the high density regime [23].

(f) *Response functions*. Finally, the response functions—specific heat per particle (at constant volume) and order-parameter susceptibility—were calculated in zero field. The corresponding analytical expressions may be found in the Appendix.

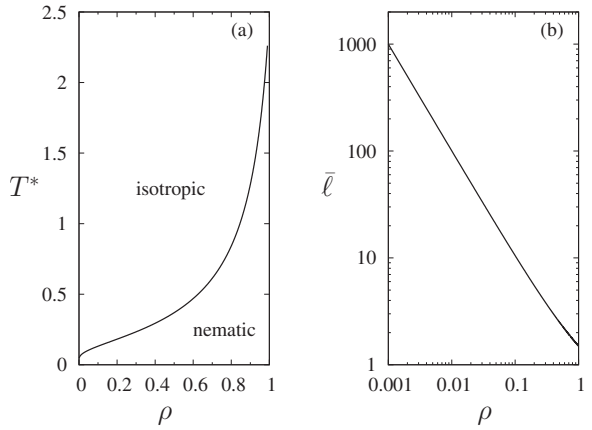

FIG. 1. (a) Phase diagram of the model. The nematic phase is stable at low temperatures and high densities. The full line is a line of critical transitions that separates regions of isotropic and nematic stability; (b) equilibrium average rod length on the transition line.

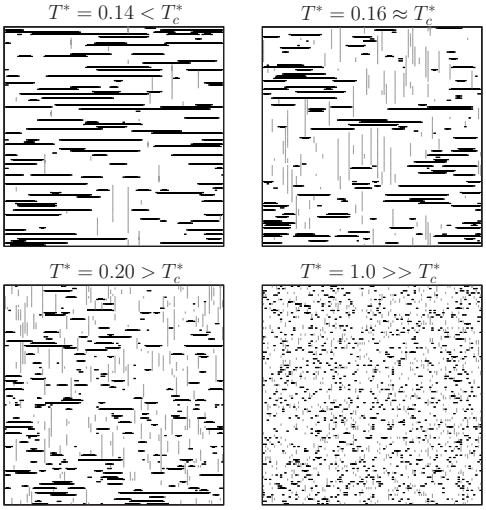

FIG. 2. Representative equilibrium configurations for the system with $\rho=0.2$ at four temperatures.

III. SELF-ASSEMBLED ZWANZIG MODEL: LATTICE SIMULATIONS

In this section, we present results of Monte Carlo simulations of the self-assembled Zwanzig model in equilibrium. We will focus on the interplay between self-assembly and the ordering transition and on a detailed comparison with the theoretical predictions. However, we will not investigate the reentrant nematic transition at high densities [22], that is not described by the theory presented above.

For simplicity, we consider a square lattice of length L with toroidal geometry (fully periodic boundary conditions) and $N=\rho L^2$ sites occupied by particles. The two bonding sites in each particle may be thought of as an internal axis that may be aligned in either of the two lattice directions. In general, the lattice symmetry imposes strong constraints on the orientational configurations of particles but this is not a problem in the Zwanzig model, where the orientational degrees of freedom are discrete. The lattice discretization of the translational degrees of freedom is not relevant in this context.

The internal energy of a particular configuration is proportional to the number of bonds between particles, where two particles are said to share a bond with energy $-\epsilon$ if they are nearest neighbors on the lattice and both axes are parallel to the lattice vector connecting them. A cluster or uninterrupted sequence of bonded particles is a rod. In the following we will use dimensionless units temperature T^* as defined in the preceding section. The lattice constant provides the unit of length. The densities are then fractions of occupied sites while rod lengths are given in terms of the number of self-assembled particles in each rod. In order to avoid cluttering the text and figures with stars we use the same symbols (ρ,ℓ) for these numbers as for the corresponding dimensional quantities.

We obtain the equilibrium properties of the system at a given temperature and density by standard Monte Carlo techniques [26]. From a random initial configuration (sites occupied with probability ρ and particle axis orientation chosen with probability $1/2$), single-particle moves are used to explore the state space in a Markov process constructed to produce a sequence of states appearing with Boltzmann probabilities in the asymptotic limit. Our choice of dynamical move consists of randomly selecting a pair of lattice sites, one occupied and one unoccupied, moving the selected particle to the unoccupied site, and rotating its axis. We use the Metropolis acceptance rule for rapid sampling of the state space. A selection of representative equilibrium configurations at four temperatures is shown in Fig. 2.

Once an equilibrium distribution of states has been obtained, the rod length density distributions, $\phi_x(\ell)$ and $\phi_y(\ell)$, are determined and thermodynamic quantities of interest are calculated from the moments of these distributions. In particular, we calculated the number of bonds, N_{bonds}, the internal energy per particle, u,

$$\frac{u}{\epsilon} = -\frac{N_{\text{bonds}}}{N} = -\left(1 - \frac{\phi}{\rho}\right), \tag{40}$$

the order parameter, Δ, the orientational densities ρ_x and ρ_y, etc. In order to obtain a large number of statistically independent measurements for calculation of expectation values, we measure the correlation time τ at each (ρ,T^*) using the autocorrelation of the order parameter $\Delta(t)$ (time is measured in units of N move attempts). Measurements are then taken at times separated by at least 2τ.

Extensive computer simulations of monodisperse rods on the square lattice have shown that the isotropic-nematic transition is in the Ising 2D universality class [20–22]. Although polydispersity may affect the nature of the transition, the theory, described previously, predicts a line of continuous transitions (see Fig. 1) and we have limited the simulation analysis to checking that the results are consistent with the working hypothesis that the nature of the transition remains unchanged.

In the following we carry out a quantitative comparison of the simulation results with the theoretical predictions described in the preceding section, at two densities $\rho=0.2$ and $\rho=0.4$.

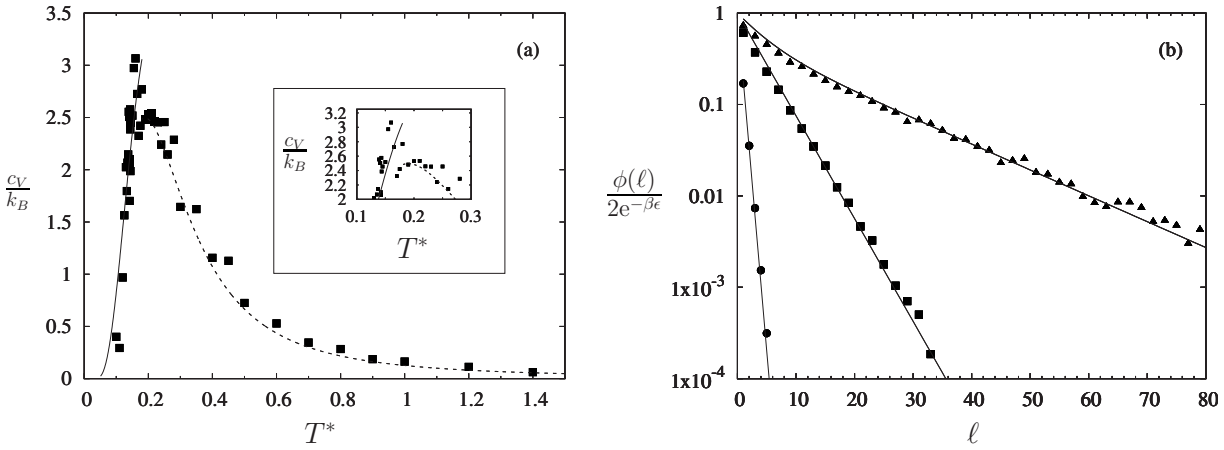

FIG. 3. Two signatures of the self-assembly process for a system with density $\rho=0.2$ and length $L=100$: The specific heat per particle as a function of temperature (a) and the total rod length density distribution (b). In the former, simulation data—as measured from the fluctuations in the internal energy—is plotted over the theoretical curve. The total rod length density distributions are shown for three temperatures $T^*=0.14$ (triangles), 0.20 (squares), and 1.0 (circles), with the theoretical curves from (35) over-plotted.

A. Self-assembly in the presence of ordering

The equilibrium behavior of the self-assembled Zwanzig model is broadly characterized by two related phenomena: the self-assembly of particles into rods and the alignment of these rods once they attain a certain average length. Both of these phenomena are illustrated in Fig. 2, where it is seen that a decrease in temperature yields longer rods and at the lowest temperature a preferred orientation is apparent.

To analyze the interplay between self-assembly and ordering, we consider the specific heat per particle which can be determined from the fluctuations of the internal energy per particle, i.e.,

$$\frac{c_V}{k_B} \equiv \frac{C_V}{k_B N} = N\frac{\langle u^2\rangle - \langle u\rangle^2}{\epsilon^2 T^{*2}}, \tag{41}$$

where C_V is the total specific heat.

At $\rho=0.2$, the theory described in the preceding section [line in Fig. 3(a)] predicts a (local) maximum for the specific heat in the isotropic phase. In single phase self-assembling systems, this maximum is used to define the bonding temperature, since it signals the onset of significant cluster formation. The theory, being mean field, also predicts a discontinuity in the specific heat at the phase transition (and not the 2D Ising logarithmic divergence, expected for an exact theory of the 2D self-assembled Zwanzig model). At the discontinuity, the specific heat is larger in the nematic phase, indicating that the isotropic nematic phase transition enhances bond formation and self-assembly.

As can be seen in Fig. 3(a), the simulation results for c_V are characterized by a broad maximum, which is rather noisy. However, careful inspection of the simulation data close to the peak [inset of Fig. 3(a)] shows the existence of a shoulder, at a temperature above that of the (global) maximum. This shoulder is described remarkably well by the theoretical bonding peak that signals the onset of self-assembly, in the isotropic phase. At lower temperatures, the ordering transition is marked by a sharper and higher maximum, distinct from the self-assembly shoulder, suggesting the expected divergence capped by finite size effects. Therefore, the simulation results confirm the prediction of the theory: Ordering enhances bonding and self-assembly.

In the case of the higher density, $\rho=0.4$, the theory predicts that the bonding temperature (signaled by a local maximum of the specific heat) shifts into the nematic phase (not shown). This result must be taken with caution, however, since the second virial coefficient approximation gives, particularly at higher densities, a poor description of the excluded volume of the system in the ordered phase that leads to an overestimate of the transition temperature. The simulation data for the specific heat at this density (not shown) were inconclusive in addressing this question.

Further evidence of the interplay between self-assembly and ordering can be seen in the length distributions for this polydisperse system. Normalized histograms showing the rod length density distributions, at $\rho=0.2$, for a number of temperatures are shown in Fig. 3(b). In the isotropic phase, the simulation data reveal a single exponential distribution as predicted by the theory (35). At the lowest temperature, $T^*=0.14$, in the nematic phase, there is evidence of a kink in the density distribution near $\ell=10$ indicating that $\phi(\ell)$ is the sum of two exponentials, $\phi_x(\ell)$ and $\phi_y(\ell)$, with $\bar{\ell}_x \neq \bar{\ell}_y$. Note that the number of long rods increases rapidly close to the bonding temperature, revealing why it is difficult to separate the onset of bonding from the ordering temperature in the simulation data.

The average rod length as a function of temperature, at two densities, $\rho=0.2$ and $\rho=0.4$, is shown in Fig. 4. The simulation data corresponds to the points with error bars and the theoretical prediction to the lines. The dashed lines are the theoretical curves, with $\Delta=0$, corresponding to the isotropic solution while the full lines, with $\Delta>0$, correspond to the nematic phase solution. The transition temperatures are indicated by vertical lines, the lower temperature being the estimate obtained from the simulation data, T^*_c, and the higher corresponding to the theoretical prediction, $T^*_{c,th}$. Above the critical temperature, there is quantitative agreement between the simulation data and the theoretical results.

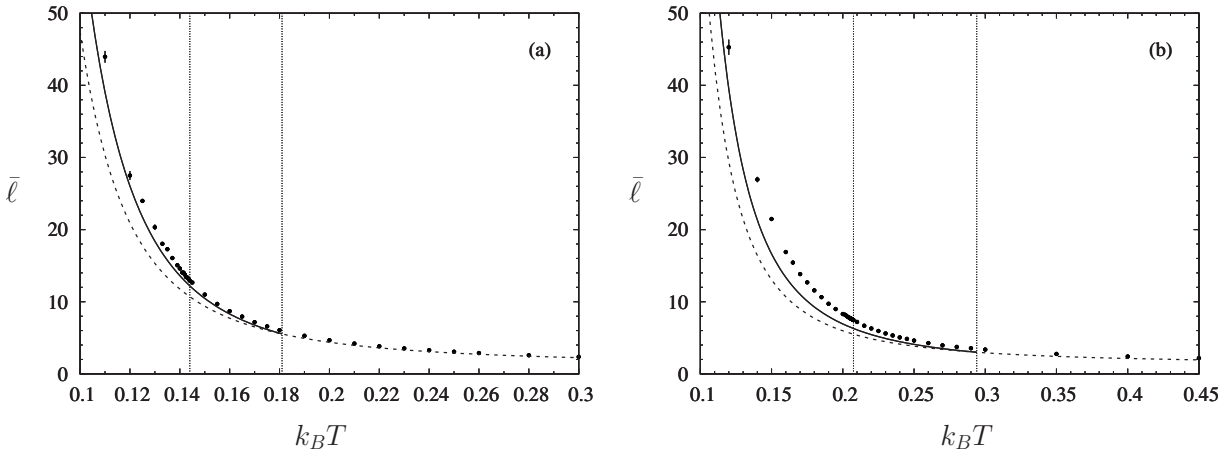

FIG. 4. Average rod length as a function of temperature from simulation data (points with error bars) and theory (lines) for two densities, $\rho=0.2$ (a) and $\rho=0.4$ (b). For the theoretical curves, the $\Delta=0$ (isotropic) solution is plotted with dashed lines and the $\Delta>0$ (nematic, $T^*<T^*_{c,th}$) solution with full lines. The temperature of the nematic transition is indicated with two vertical lines, corresponding to the theoretical prediction $T^*_{c,th}$ and that obtained from the simulation T^*_c.

Below the critical temperature, the nematic phase solution is still in good agreement with the numerical results for the system at the lower density, $\rho=0.2$, but significant differences are observed for the high density system, $\rho=0.4$. Even in this case, the theory predicts that the average rod length increases in the nematic phase, when compared to the isotropic solution, in line with the simulation data. In this sense we conclude that ordering enhances bonding as the equilibrium rods are longer than they would have been in the isotropic phase.

B. Isotropic-nematic phase transition

We now turn to the calculation of the critical isotropic-nematic transition. Finite size effects are unavoidable when self-assembly is present. In order to minimize them we avoided simulating systems where the rod length approaches the spanning length of the box. For a given density ($\rho=0.2$ and $\rho=0.4$) and simulation box ($L=100$), this sets a lower bound on the temperature for which results may be obtained. For both densities, we have limited production runs to temperatures $T^*>0.11$ that guarantee $\bar{\ell}<L/2$. A second finite-size effect, relevant in the calculation of the order parameter, is that of global fluctuations near the nematic critical temperature, T^*_c. In infinite systems at subcritical temperatures, there is a preferred nematic orientation that remains constant, but in finite systems the probability for a global fluctuation is non-negligible. In long production runs, the mean value of the order parameter Δ becomes zero below the critical temperature as a result of these fuctuations. To avoid this, we used the magnitude of Δ, which accounts for the small non-zero values of the order parameter in the isotropic phase. Although the data presented below was obtained for a single lattice size ($L=100$), we have checked the results on larger lattices and observed, for example, less than a 10% change in the nematic transition temperature. Finally, we assume that the isotropic-nematic transition for the polydisperse 2D Zwanzig model remains in the Ising 2D universality class. A rigorous finite size scaling analysis, required for the investigation of the effect of polydispersity on the nature of the transition, is left for future work.

The order parameter $|\Delta|$ as a function of temperature, is shown in Fig. 5 for the two systems, $\rho=0.2$ (a) and $\rho=0.4$ (b). The theoretical curves are over-plotted as dashed lines

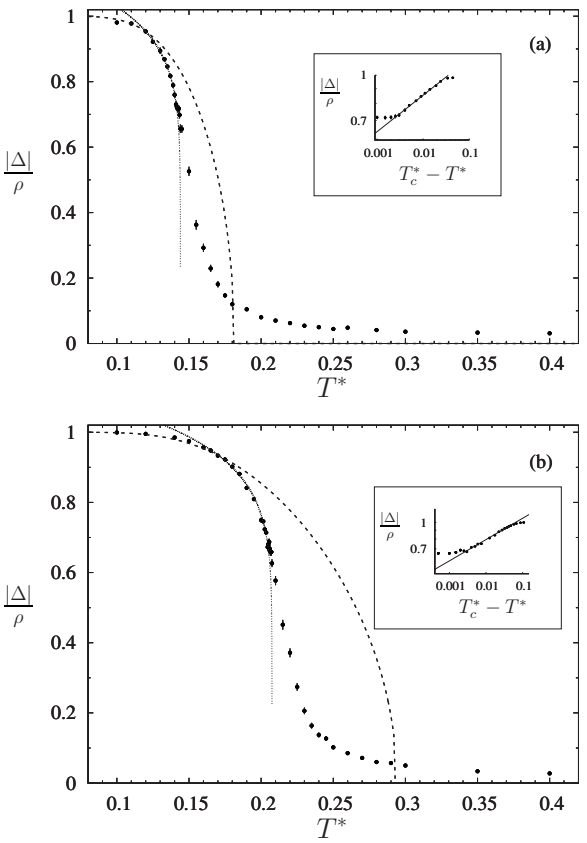

FIG. 5. Plot of the orientational order parameter Δ as a function of temperature for $\rho=0.2$ (a) and $\rho=0.4$ (b) with theoretical curves over-plotted (dashed). The light dashed lines are the best fits to $(T^*_c-T^*)^{1/8}$, where $T^*_c[\rho=0.2]=0.144$ and $T^*_c[\rho=0.4]=0.2075$.

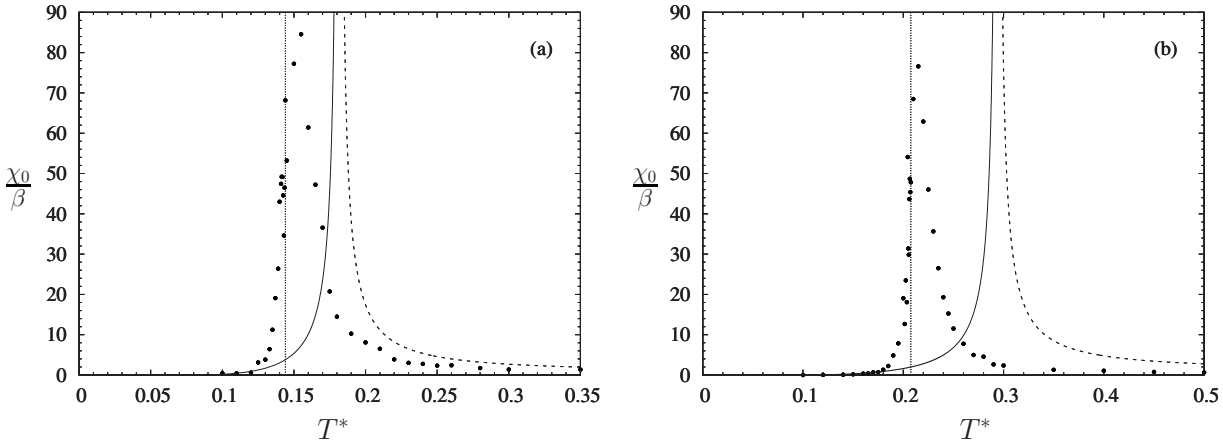

FIG. 6. Fluctuations of the order parameter $|\Delta|$ as a function of temperature for densities $\rho=0.2$ (a) and $\rho=0.4$ (b). Vertical lines indicate the estimated T_c^*, as determined by the fit in the insets of Fig. 5.

and it is clear that the theory overestimates the transition temperature in both cases, with the result for the high density system being almost 30% higher. We estimate the transition temperature, by fitting the simulation data with an Ising order-parameter scaling of the form $(T_c^*-T^*)^{1/8}$ [26]. This yields the values $T_c^*=0.144$ for $\rho=0.2$ and $T_c^*=0.2075$ for $\rho=0.4$. The light dashed lines are the best fits to $(T_c^*-T^*)^{1/8}$, while the insets show that at temperatures not too close to the transition, the Ising scaling hypothesis for the order parameter is consistent with the simulation data.

As a final check on the continuity of the transition we have calculated the fluctuations of the order parameter. The zero field susceptibility per particle, χ_0, is [26]

$$\beta^{-1}\chi_0 = \frac{N}{\rho^2}[\langle\Delta^2\rangle - \langle\Delta\rangle^2], \tag{42}$$

and is expected to diverge at the transition, more strongly than the specific heat [26]. The simulation data corresponding to the order parameter $|\Delta|$ are plotted as a function of temperature in Fig. 6, for the two densities $\rho=0.2$ (a) and $\rho=0.4$ (b). The vertical lines indicate the estimates of T_c^*, as determined by the fit displayed in the insets of Fig. 5. The theoretical results, obtained from Eq. (A11) are over-plotted in Fig. 6. Note that the range of temperatures plotted here is comparable to that of the inset in Fig. 3(a). The transition is clearly signalled by the sharp maximum in the susceptibility, that occur at temperatures slightly above the estimates for the infinite system critical temperatures, T_c^*. The rounding off of the divergence as well as the shift in the peak positions are in line with finite size scaling theory [26] and confirm the continuity of the transition. We note that the shift in the peak position is larger for the lower density system, where the rods are longer, rendering the box length effectively smaller.

IV. CONCLUSIONS

We have studied the isotropic-nematic transition in a system of self-assembling rods as part of the general effort to develop a deeper understanding of self-assembly. A long term goal is to rationalize the behavior of other systems such as semiflexible polymeric systems with a small fraction of functionalized monomers as well as that of particles with lock-and-key type of interactions, encountered in biological self-assembly [27–29].

We have investigated the influence of directional or bonding interactions on the structure and phase diagram of a model fluid close to an ordering transition, focusing on the interplay between bonding and nematic ordering in a self-assembled Zwanzig model in 2D. The simplicity of the model allowed a generalization of the theory of associating fluids that describes quantitatively the rod length density distributions and the average rod lengths, in the isotropic as well as in the nematic phase. The average rod length was found to be longer in the nematic phase, in comparison with the isotropic length, and we conclude that nematic ordering enhances bonding.

Comparison with Monte Carlo simulations, on the square lattice, revealed that the location of the isotropic-nematic transition is overestimated by the theory at densities as low as $\rho=0.2$ and that results for higher densities are not reliable. As higher-order virial coefficients for this model are known exactly, significant improvement is possible at the expense of the simplicity of the theoretical treatment.

One of the two response functions investigated, the specific heat, was shown to exhibit nontrivial structure at the onset of self-assembly close to the isotropic-nematic transition. The self-assembly process and the ordering transition occur separately but close in temperature, at $\rho=0.2$. The mean-field theory was proved quite accurate in the description of the bonding contribution to the specific heat but less so in the description of the specific heat at the isotropic-nematic transition.

The question of whether ordering enhances bonding may be worth investigating with a more accurate theory, as the specific heat simulation data is difficult to interpret. The theory presented here predicts that the bonding temperature shifts to the nematic phase, at $\rho=0.4$, but due to the overestimate of the ordering temperature at this density this result should be taken with caution. The simulation data for the specific heat at $\rho=0.4$ was inconclusive and the shift of the bonding temperature to the nematic phase at high densities is

an open question. A finite size scaling analysis seems to be required to allow the separation of the bonding and ordering contributions to c_V as well as to investigate the effect of polydispersity on the nature of the isotropic-nematic transition, both of which will be addressed in future work.

The results of this work aim to contribute to the ellucidation of the collective properties of patchy colloids using simple models. It has been shown that in systems with a small number of bonding sites the structure and phase diagram may change drastically. In particular, if the number of identical bonding sites per particle is reduced to two the critical density vanishes and gel-like states, with an open network structure, become accessible at low packing fractions [6]. We have addressed that limit for stiff chains and, shown that, if the clusters are sufficiently stiff, nematic ordering will preempt the access to the gel phase.

ACKNOWLEDGMENTS

Financial support from the Foundation of the University of Lisbon and the Portuguese Foundation for Science and Technology (FCT) under Contracts No. POCI/FIS/55592/2004 and No. POCTI/ISFL/2/618 is gratefully acknowledged. B.P.H. acknowledges FCT for Grant No. SFRH/BPD/38976/2007.

APPENDIX

The isotropic-nematic critical line and the response functions—specific heat and susceptibility in zero field, c_V and χ_0—are calculated most easily in terms of the auxiliary variables,

$$X = z\exp(\tilde{\Delta}), \tag{A1}$$

$$Y = z\exp(-\tilde{\Delta}). \tag{A2}$$

These variables are written as implicit functions of (ρ,Δ,T), using the equations of state (29) and (30),

$$\rho + \Delta = \exp(-\beta\epsilon)\frac{2X}{(1-X)^2}, \tag{A3}$$

$$\rho - \Delta = \exp(-\beta\epsilon)\frac{2Y}{(1-Y)^2}. \tag{A4}$$

This formulation allows a straightforward calculation of the derivatives of X and Y,

$$\left(\frac{\partial X}{\partial \Delta}\right)_{\rho,T} = \exp(\beta\epsilon)\frac{(1-X)^3}{2(1+X)}, \tag{A5}$$

$$\left(\frac{\partial Y}{\partial \Delta}\right)_{\rho,T} = -\exp(\beta\epsilon)\frac{(1-Y)^3}{2(1+Y)}, \tag{A6}$$

$$\left(\frac{\partial X}{\partial T}\right)_{\rho,\Delta} = -\frac{\epsilon}{k_B T^2}\frac{X(1-X)}{1+X}, \tag{A7}$$

$$\left(\frac{\partial Y}{\partial T}\right)_{\rho,\Delta} = -\frac{\epsilon}{k_B T^2}\frac{Y(1-Y)}{1+Y}, \tag{A8}$$

required in various quantities of interest, as listed below.

The calculation of the isotropic-nematic transition line and the suscpetibility are most easily carried out, using (A1) and (A2) in (25) to write the external field h, as a function of (ρ,Δ,T),

$$\beta h = \frac{1}{2}\left(\ln\frac{X}{Y} - \Delta\right). \tag{A9}$$

The inverse order-parameter susceptibility is

$$\beta\chi_0^{-1} = \left(\frac{\partial \beta h}{\partial \Delta}\right)_{\rho,T} = \left(\frac{\partial \beta h}{\partial \Delta}\right)_{X,Y} + \left(\frac{\partial \beta h}{\partial X}\right)_{Y,\Delta}\left(\frac{\partial X}{\partial \Delta}\right)_{\rho,T} + \left(\frac{\partial \beta h}{\partial Y}\right)_{X,\Delta}\left(\frac{\partial Y}{\partial \Delta}\right)_{\rho,T}, \tag{A10}$$

which, using (A1)–(A6) and (A9), becomes, in zero field,

$$\beta\chi_0^{-1} = \frac{1}{2}\left(\frac{1-X}{(1+X)(\rho+\Delta)} + \frac{1-Y}{(1+Y)(\rho-\Delta)} - 1\right). \tag{A11}$$

This equation was used to calculate the theoretical susceptiblity plotted in Fig. 6. In the isotropic phase ($h=0$ and $\Delta=0$), $X=Y=z$, and the previous equation becomes

$$\left(\frac{\partial \beta h}{\partial \tilde{\Delta}}\right)_{\rho} = 1 - \frac{\rho}{2}\frac{1+z}{1-z}, \tag{A12}$$

the zero of which defines the isotropic-nematic transition line.

The internal energy per particle (40) is simply written as

$$u = -\epsilon\left[1 - \frac{\exp(-\beta\epsilon)}{\rho}\left(\frac{X}{1-X} + \frac{Y}{1-Y}\right)\right], \tag{A13}$$

and the specific heat per particle is

$$c_V = \left(\frac{\partial u}{\partial T}\right)_{\rho,h} = \left(\frac{\partial u}{\partial T}\right)_{\rho,\Delta} + \left(\frac{\partial u}{\partial \Delta}\right)_{\rho,T}\left(\frac{\partial \Delta}{\partial T}\right)_{\rho,h}, \tag{A14}$$

where,

$$\left(\frac{\partial \Delta}{\partial T}\right)_{\rho,h} = -\frac{\left(\frac{\partial h}{\partial T}\right)_{\rho,\Delta}}{\left(\frac{\partial h}{\partial \Delta}\right)_{\rho,T}}. \tag{A15}$$

All these derivatives can be expressed in terms of (A5)–(A8), and of the derivatives of u with respect to X, Y, and T. The specific heat in zero field is then,

$$\rho T^{*2} k_B^{-1} c_V = \exp\left(-\frac{1}{T^*}\right)\left(\frac{X^2}{1-X^2} + \frac{Y^2}{1-Y^2}\right) + \frac{1}{2}\left(\frac{[F(X)-F(Y)]^2}{\frac{F(X)}{\rho+\Delta} + \frac{F(Y)}{\rho-\Delta} - 1}\right), \tag{A16}$$

where $F(x)=\frac{1-x}{1+x}$. This expression was used to calculate the theoretical specific heat plotted in Fig. 3(a). At fixed values of ρ, T, and h, X, Y, and Δ (or z, $\tilde{\Delta}$, and Δ) are obtained by solving the equations of state (A3), (A4), and (A9). All other equilibrium quantities of interest may be calculated from them. Note that $h=0$ is equivalent to $\tilde{\Delta}=\Delta$ and that in the isotropic phase ($h=0$ and $\Delta=0$), $X=Y=z$ yielding simpler expressions for the thermodynamic and structural properties.

[1] A. van Blaaderen, Nature (London) **439**, 545 (2006).
[2] M. S. Wertheim, J. Stat. Phys. **35**, 19 (1984).
[3] M. S. Wertheim, J. Stat. Phys. **35**, 35 (1984).
[4] E. Bianchi, J. Largo, P. Tartaglia, E. Zaccarelli, and F. Sciortino, Phys. Rev. Lett. **97**, 168301 (2006).
[5] F. Sciortino, Eur. Phys. J. B **64**, 505 (2008).
[6] G. Foffi and F. Sciortino, J. Phys. Chem. B **111**, 9702 (2007).
[7] F. Sciortino, E. Bianchi, J. F. Douglas, and P. Tartaglia, J. Chem. Phys. **126**, 194903 (2007).
[8] L. Onsager, Ann. N.Y. Acad. Sci. **51**, 627 (1949).
[9] Z. X. Zhang and J. S. van Duijneveldt, J. Chem. Phys. **124**, 154910 (2006).
[10] P. A. Buining and H. N. W. Lekkerkerker, J. Phys. Chem. **97**, 11510 (1993).
[11] A. Speranza and P. Sollich, J. Chem. Phys. **117**, 5421 (2002).
[12] R. Zwanzig, J. Chem. Phys. **39**, 1714 (1963).
[13] N. Clarke, J. A. Cuesta, R. Sear, P. Sollich, and A. Speranza, J. Chem. Phys. **113**, 5817 (2000).
[14] H. H. Wensink and G. J. Vroege, J. Chem. Phys. **119**, 6868 (2003).
[15] A. Speranza and P. Sollich, Phys. Rev. E **67**, 061702 (2003).
[16] A. Speranza and P. Sollich, J. Chem. Phys. **118**, 5213 (2003).
[17] J. P. Straley, Phys. Rev. A **4**, 675 (1971).
[18] D. Frenkel and R. Eppenga, Phys. Rev. A **31**, 1776 (1985).
[19] P. van der Schoot, J. Chem. Phys. **106**, 2355 (1997).
[20] D. A. Matoz-Fernandez, D. H. Linares, and A. J. Ramirez-Pastor, J. Chem. Phys. **128**, 214902 (2008).
[21] D. A. Matoz-Fernandez, D. H. Linares, and A. J. Ramirez-Pastor, Europhys. Lett. **82**, 50007 (2008).
[22] A. Ghosh and D. Dhar, Europhys. Lett. **78**, 20003 (2007).
[23] A. J. Masters, J. Phys.: Condens. Matter **20**, 283102 (2008).
[24] J. M. Tavares, J. J. Weis, and M. M. Telo da Gama, Phys. Rev. E **73**, 041507 (2006).
[25] P. I. C. Teixeira, J. M. Tavares, and M. M. Telo da Gama, J. Phys.: Condens. Matter **12**, R411 (2000).
[26] M. E. J Newman and G. T. Barkema, *Monte Carlo Methods in Statistical Physics* (Clarendon, Oxford, 1999).
[27] H. Fraenkel-Conrat and R. C. Williams, Proc. Natl. Acad. Sci. U.S.A. **41**, 690 (1955).
[28] Z. Zhang and S. C. Glotzer, Nano Lett. **4**, 1407 (2004).
[29] K. Van Workum and J. F. Douglas, Phys. Rev. E **73**, 031502 (2006).